Research Article

Chunyuan Lu and Zongyong Lou*

Numerical study of static pressure on the sonochemistry characteristics of the gas bubble under acoustic excitation

https://doi.org/10.1515/phys-2023-0124
received June 15, 2023; accepted October 03, 2023

Abstract: The extreme environment formed during bubble collapse can cause a series of chemical reactions inside the bubble, and multiple products (*i.e.*, $^{\cdot}OH$, $H^{\cdot}$, O, H_2, and $HO_2^{\cdot}$, *etc.*) are produced, which is called sonochemistry. In this study, a new model is used to predict the sonochemistry characteristics inside an oxygen bubble oscillating in water. The influences of static pressure, ultrasonic frequency, and the equilibrium radius on the temperature inside the bubble and the yields of chemical products are analyzed. The numerical calculation results are obtained during bubble oscillations under a steady state, which is different from the previous studies that focus on the sonochemical characteristics at the bubble collapse. Numerical studies show that with the change in the equilibrium radius, the maximum bubble temperature fluctuates drastically, and the maximum yields of H_2 and $^{\cdot}OH$ show a Gaussian curve trend. The cavitation activity corresponding to the equilibrium radius depends on the combination of static pressure and ultrasonic frequency.

Keywords: bubble, sonochemistry, steady state, static pressure, equilibrium radius

1 Introduction

The growth, contraction, and collapse of the bubbles caused by ultrasonic radiation in liquid are called acoustic cavitation, which is widely applied in many fields such as ultrasonic cleaning [1], water treatment [2], assisted surfactant extraction [3], and ultrasonic diagnosis [4]. The concept of sonochemistry emerged from the phenomenon of cavitation, which refers to the collapse of the bubbles resulting in an internal temperature of several thousand Kelvin and pressure of several hundred atmospheres. Under this extreme environment, the water vapor water inside the bubble can be decomposed forming $^{\cdot}OH$, $H^{\cdot}$, O, $HO_2^{\cdot}$, H_2O_2, and H_2, *etc*.

The study of cavitation began in 1917 when Raleigh established the first mathematical model to describe the characteristics of a spherical cavity in incompressibility [5]. In 1944, Weiss [6] observed the formation of $^{\cdot}OH$ and $H^{\cdot}$ in the water radiated by ultrasound. Parke and Taylor [7] demonstrated for the first time the formation of $^{\cdot}OH$ in water. The production rate of $^{\cdot}OH$ in the sonochemistry experiment of a single bubble was measured by Didenko and Suslick [8]. Sonochemical effects have been used in many fields. For example, the degradation and isomerization of 3- and 4-*O*-caffeoylquinic acid were facilitated by ultrasonic treatment [9]. Organic pollutants and pathogenic microorganisms in water can be eliminated in an ultrasound field, which was enhanced by dual-frequency ultrasound [10]. Compared to the myofibrillar protein solution without ultrasound treatment, the surface hydrophobicity, emulsification properties, carbonyl groups, and intrinsic fluorescence intensity of the ultrasound-treated myofibrillar protein solution were increased [11]. The emulsifying features, structure, and interfacial features of oxidized soybean protein aggregates were optimized by ultrasonic treatment [12]. In terms of hydrogen energy production, ultrasonic-assisted electrochemical hydrogen production can increase the overall efficiency by 10–15% [13]. Another study by the same research group showed that ultrasonic-assisted water electrolysis can increase hydrogen production efficiency by 4.5% [14].

In 1993, Kamath *et al.* [15] published the first paper on the numerical calculation of sonochemistry. In the following 30 years, the theoretical models of sonochemistry have been greatly developed. Heat conduction inside and outside the bubble, unbalanced evaporation and

* **Corresponding author: Zongyong Lou,** Department of Thermal Engineering, Hebei Petroleum University of Technology, Chengde, China, e-mail: louzongyong112@163.com
Chunyuan Lu: School of Mechano-Electronic Engineering, Suzhou Vocational University, Suzhou, China

condensation of water vapor at the bubble wall, chemical reactions inside the bubble, and changes in physical properties of the liquid (such as saturated vapor pressure, surface tension, latent heat of evaporation, thermal conductivity and viscosity) were successively considered [16–21]. Specifically, Kalmár *et al.* [21] introduced a state-of-the-art chemical mechanism to suitably describe chemical processes inside a spherical bubble with oxygen and water vapor.

In the above models, the effects of ultrasonic amplitude, frequency, liquid temperature and dissolved gas properties on the sonochemistry were well revealed. Static pressure has an important effect on the cavitation such as the cavitation threshold and the inertial cavitation intensity, but the study of the effect of static pressure on the sonochemistry is very limited. Yasui *et al.* [16] and Merouani *et al.* [17] studied the effects of ultrasonic amplitude and static pressure on oxidant yields when the excitation frequencies were 140 and 300 kHz and the equilibrium radius of the bubble was a fixed value, respectively, and found that the optimal static pressure value varied with the ultrasonic amplitude. Experimental studies showed that the equilibrium radius of the bubble is within a certain range after the generation of cavitation [18]. Dehane *et al.* [19] analyzed the influence of static pressure on the output of $^{\cdot}OH$, $H^{\cdot}$, O, $HO_2^{\cdot}$, and H_2 under high-frequency (355 and 1,000 kHz) excitation, but the authors did not give the corresponding optimal equilibrium radius under different static pressures. Nevertheless, previous studies [16,17,19] focused on the influence of static pressure on the sonochemical characteristics during bubble collapse, and the bubble collapse time is far less than the time of the oscillations during a steady state. Therefore, it is necessary to analyze the influence of static pressure and bubble equilibrium radius on the sonochemical characteristics, especially the optimal equilibrium radius corresponding to H_2 and $^{\cdot}OH$ amounts during bubble oscillations of steady state. The research results can better guide the experimental research and application of sonochemistry.

2 Model and methods

The model used in this study is proposed by Kalmár *et al.* [21] introducing a state-of-the-art chemical mechanism. The bubble always remains spherical and its center is fixed during oscillations neglecting the interaction between bubbles. The physical processes considered are as follows: heat conduction inside and outside the bubble, non-equilibrium evaporation and condensation of water vapor at the bubble wall, and chemical reactions inside the bubble. The radial motion of the bubble is described by the Keller–Miksis equation [17,18]:

$$\begin{aligned}&\rho\left(1-\frac{\dot{R}}{c}\right)R\ddot{R}+\frac{3}{2}\rho\dot{R}^2\left(1-\frac{1}{3}\frac{\dot{R}}{c}\right)\\&=\left(1+\frac{\dot{R}}{c}\right)[p_{\text{ext}}(R,t)-p_\infty(t)]+\frac{R}{c}\frac{\mathrm{d}}{\mathrm{d}t}[p_{\text{ext}}(R,t)\\&\quad-p_\infty(t)],\end{aligned}\tag{1}$$

where R is the instantaneous radius of the bubble, t is the time, the overdot denotes the time derivative, ρ is the density of the liquid, and c is the speed of sound in the liquid. The pressure at infinity consists of static pressure and dynamic pressure, expressed as follows:

$$p_\infty(t)=P_\infty-P_{\text{A}}\sin(2\pi ft),\tag{2}$$

where P_∞ is the static pressure, and P_{A} and f are the amplitude and frequency of the external acoustic excitation, respectively. The liquid pressure acting on the bubble wall is as follows:

$$p_{\text{ext}}(R,t)=p_{\text{in}}-\frac{2\sigma}{R}-\frac{4\mu}{R}\dot{R},\tag{3}$$

where p_{in} is the pressure inside the bubble, σ is the surface tension coefficient of the liquid, and μ is the viscosity of the liquid.

The pressure of the mixed gas inside the bubble is described by the state equation of ideal gas [21], which is expressed as follows:

$$p_{\text{in}}=MR_{\text{g}}T,\tag{4}$$

where M is the total concentration of the mixture, R_{g} is the universal gas constant, and T is the temperature inside the bubble:

$$\dot{T}=\frac{-p_{\text{in}}\dot{V}+\sum\dot{Q}}{n_{\text{t}}\bar{C}_{\text{v}}},\tag{5}$$

where $\sum\dot{Q}$ is the total heat, including heat transfer and chemical reaction heat. n_{t} is the total molar mass of the mixture and $\bar{C}_{\text{v}}$ is the average molar heat capacity of the mixture at a constant volume, which is calculated based on the NASA chemical equilibrium code [21].

Heat transfer can be expressed as [20,21]

$$\dot{Q}_{\text{th}}=A\bar{\lambda}\frac{\partial T}{\partial r}\bigg|_{r=R}\approx A\bar{\lambda}\frac{T_\infty-T}{l_{\text{th}}},\tag{6}$$

$$l_{\text{th}}=\min\left\{\frac{R}{\pi},\sqrt{\frac{R\chi}{\dot{R}}}\right\},\tag{7}$$

where A is the surface area of the bubble, $\bar{\lambda}$ and χ are the average thermal conductivity and thermal diffusivity of the gas mixture inside the bubble, respectively, T_∞ is the

liquid temperature at infinity, and l_{th} is the thickness of the thermal boundary layer.

Reversible reactions involving K chemical substances inside the bubble are expressed as follows [15–20]:

$$\sum_{k=1}^{K} \upsilon_{ki}^{f} \chi_k \leftrightarrow \sum_{k=1}^{K} \upsilon_{ki}^{r} \chi_k \, (k = 1, \ldots, K), \tag{8}$$

where υ_{ki} are the stoichiometric coefficients, χ_k is the chemical symbol for the kth species, and superscripts f and r represent forward and reverse stoichiometric coefficients, respectively. The subscript i is the type of chemical reaction and I is the total number of chemical reactions.

The expression of the net reaction rate is as follows [15–20]:

$$q_i = k_{f_i} \prod_{k=1}^{K} c_k^{\upsilon_{ki}^{f}} - k_{r_i} \prod_{k=1}^{K} c_k^{\upsilon_{ki}^{r}}, \tag{9}$$

where c_k is the molar concentration of the kth species, and k_{f_i} and k_{r_i} are the forward and reverse rate constants for the ith reaction, respectively. The forward rate coefficient calculated by the extended Arrhenius equation is given as [15–20]

$$k_{fi} = A_{fi} T^{b_{fi}} \exp\left(-\frac{E_{af_i}}{R_g T}\right), \tag{10}$$

where A_{fi} is the pre-exponential, b_f is the temperature exponent, and E_{af_i} is the activation energy. The reverse rate constant is not the same as that in most references [15–20], and the calculation method can be found in the study of Kalmár *et al.* [21].

The total net chemical reaction heat [21] is

$$\dot{Q}_h = -\sum_{k=1}^{K} H_k \dot{\omega}_k, \tag{11}$$

where H_k and $\dot{\omega}_k$ are the enthalpy of formation and the production rate of each species, respectively.

The net condensation for unit time and area is [21]

$$\dot{n}_{net} = \dot{n}_{eva} - \dot{n}_{con} = \frac{\alpha_M p_v^*}{W_{H_2O}\sqrt{2\pi R_v T_\infty}} - \frac{\alpha_M p_{H_2O}}{W_{H_2O}\sqrt{2\pi R_v T}}, \tag{12}$$

where $\dot{n}_{eva}$ is the rate of evaporation, $\dot{n}_{con}$ is the rate of condensation, α_M is the accommodation coefficient for evaporation, p_v^* is the saturated vapor pressure, R_v is the specific gas constant of water, W_{H_2O} is the molecular weight of water, and p_{H_2O} is the partial pressure of water vapor and is given as

$$p_{H_2O} = \frac{N_{H_2O}}{N_t} p_{in}, \tag{13}$$

where N_{H_2O} is the amount of water vapor inside the bubble.

The concentration change of the kth component is [21]

$$\dot{c}_k = \dot{\omega}_k - c_k \frac{\dot{V}}{V}, \tag{14}$$

where V is the instantaneous volume of the bubble.

Due to evaporation and condensation, the concentration of water vapor needs to be treated differently [21]:

$$\dot{c}_{H_2O} = \dot{\omega}_{H_2O} - c_{H_2O} \frac{\dot{V}}{V} + \dot{n}_{net} \frac{A}{V}. \tag{15}$$

In this study, the interior of the bubble initially contains pure oxygen and water vapor. For the possible chemical reactions inside an oxidant bubble, see the study of Kalmár *et al.* [21]. The equations described above constitute a closed system solved by using the ODE15s solver in MATLAB, and both the absolute tolerance and relative tolerance are 1×10^{-10}. The initial conditions are as follows: $R(0) = R_0$, $\dot{R}(0) = 0$, and $T(0) = T_\infty$. For the calculation method of initial concentrations of oxygen and water vapor, see the study of Kalmár *et al.* [21]. If not specified, the following constants are used in numerical calculations [15–21]: T_∞ = 300 K; P_∞ = 1 atm; ρ = 1,000 kg/m^3; σ = 0.072 N/m; c = 1,480 m/s; μ = 1.005 × 10^{-3} Pa s; and α_M = 0.5 m/s.

3 Results and discussion

Figure 1 shows the obtained results for P_A = 1.8 atm, f = 100 kHz, P_∞ = 1 atm and R_0 = 8 μm for the first 16 excitation cycles. In chart (a), the bubble begins to expand when there is negative pressure. With the increase of the absolute value of the negative pressure, the bubble expands rapidly and reaches the maximum radius until the positive pressure is reached. Under the action of the positive pressure, the bubble rapidly compresses to the minimum radius and the internal temperature reaches a maximum. At this time, the pressure inside the bubble is higher than the liquid pressure, and the bubble expands again. The bubble oscillates several times, and due to the attenuation of viscosity, thermal, and compressibility of the liquid, the local maximum bubble radius decreases and tends to the equilibrium radius until the onset of the negative pressure. The bubble temperature increases sharply at collapse causing H_2O molecules to dissociate and produce a variety of chemical products (e.g. $^{\cdot}OH$, $H^{\cdot}$, O, $HO_2^{\cdot}$, H_2, and H_2O_2 in chart (b)). The variety of product yields inside the bubble at the second collapse is presented in chart (c). It can be observed that, at the collapse phase, the decomposition of water vapor leads to a sharp decrease in H_2O. Meanwhile, the amounts of

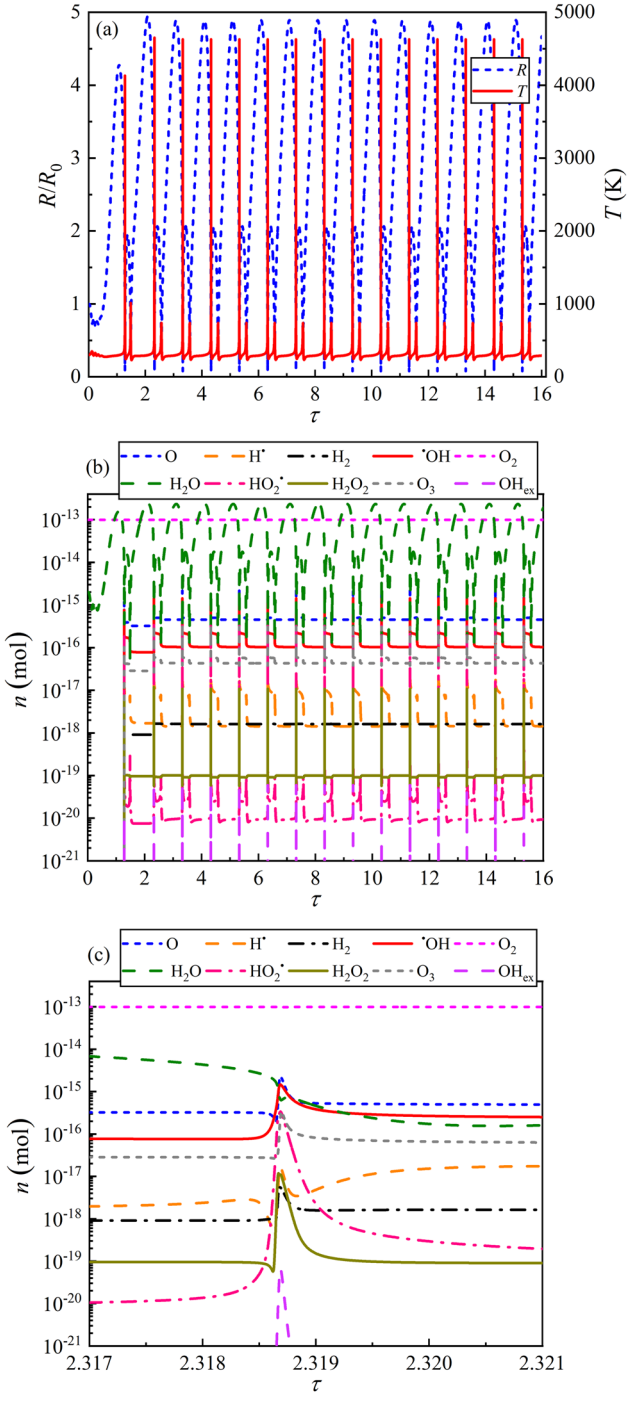

Figure 1: The calculated bubble radius (blue line), temperature (red line) in chart (a), molar yields of different products in chart (b), and product yields at the second bubble collapse in chart (c) with P_A = 1.8 atm, f = 100 kHz, P_∞ = 1 atm, and R_0 = 8 μm. The time axes are in dimensionless form: $\tau = t \cdot f$.

other chemicals increase drastically. For instance, the amount of ˙OH and $HO_2^{\cdot}$ increases by two and four orders of magnitude (from 7.62×10^{-17} to 1.46×10^{-15} mol and from 1.07×10^{-20} to 3.36×10^{-16} mol), respectively. After the end of the bubble collapse phase, molar yields of different products are basically constant, which can be clearly seen in chart (b). During the slow expansion of the bubble, chemical production and consumption, including the diffusion of free radicals into the liquid, are in dynamic equilibrium.

As shown in chart (b) in Figure 1, there is a transient process, and the molar yields of chemical products increase in the first few evolution cycles until they reach stable values (*i.e.*, dynamic equilibrium). For example, the molar yield of ˙OH (red solid line) is 0, 7.79×10^{-17}, 2.90×10^{-16}, and 4.53×10^{-16} mol during the first four cycles, respectively. After this transient process, all molar yields of chemical products remain constant during bubble expansion. Similar results were obtained in the study of Kalmár *et al.* [20]. In most studies [17–19], the chemical production at the bubble collapse is used to establish the cavitation activity, and the accuracy of the results needs to be further explored. During an acoustic cycle, compared with the time that the dynamic equilibrium state is maintained, the time that the production during bubble collapse is transient. In this study, the calculation time is 30 acoustic cycles. During the last four cycles, the maximum value of the temperature is extracted, and the molar amount of chemical product corresponding to the maximum bubble radius is the sampling point. According to the results in the studies of Kalmár *et al.* [20,21], the transient process has been safely removed in this study.

As shown in charts (b) and (c) in Figure 1, many chemical products are generated, such as ˙OH, H˙, O, $HO_2^{\cdot}$, H_2O_2, and H_2 which are the basis for the applications of sonochemistry in wastewater treatment, drinking water disinfection energy field, and so on. H_2O_2 is effective against bacteria, yeast, microalgae, and viruses [2]. ˙OH is critical to the efficiency of ultrasonic oxidation processes [22]. As a strong oxidant, O can exist stably in an aqueous solution and can diffuse in water to oxidize phenol without causing other water decomposition reactions [23]. As a promising renewable energy source, H_2 has attracted attention around the world [13,14]. Therefore, in the following analysis, the production of ˙OH and H_2 during the steady state is used to evaluate the bubble activity, and the influence of static pressure and equilibrium radius on ˙OH and H_2 production is also analyzed.

The variation in the maximum bubble temperature (T_{max}) during the steady state as the function of the bubble equilibrium radius (R_0) under different static pressures and ultrasonic frequencies (140, 355, and 515 kHz) is shown in Figure 2. The case of 140 kHz excitation as shown in Figure 2(a) is first analyzed. With the increase of R_0, T_{max} fluctuates drastically, and there are several local maximum and minimum values. At various R_0 values, T_{max} has a maximum value, but the equilibrium radius

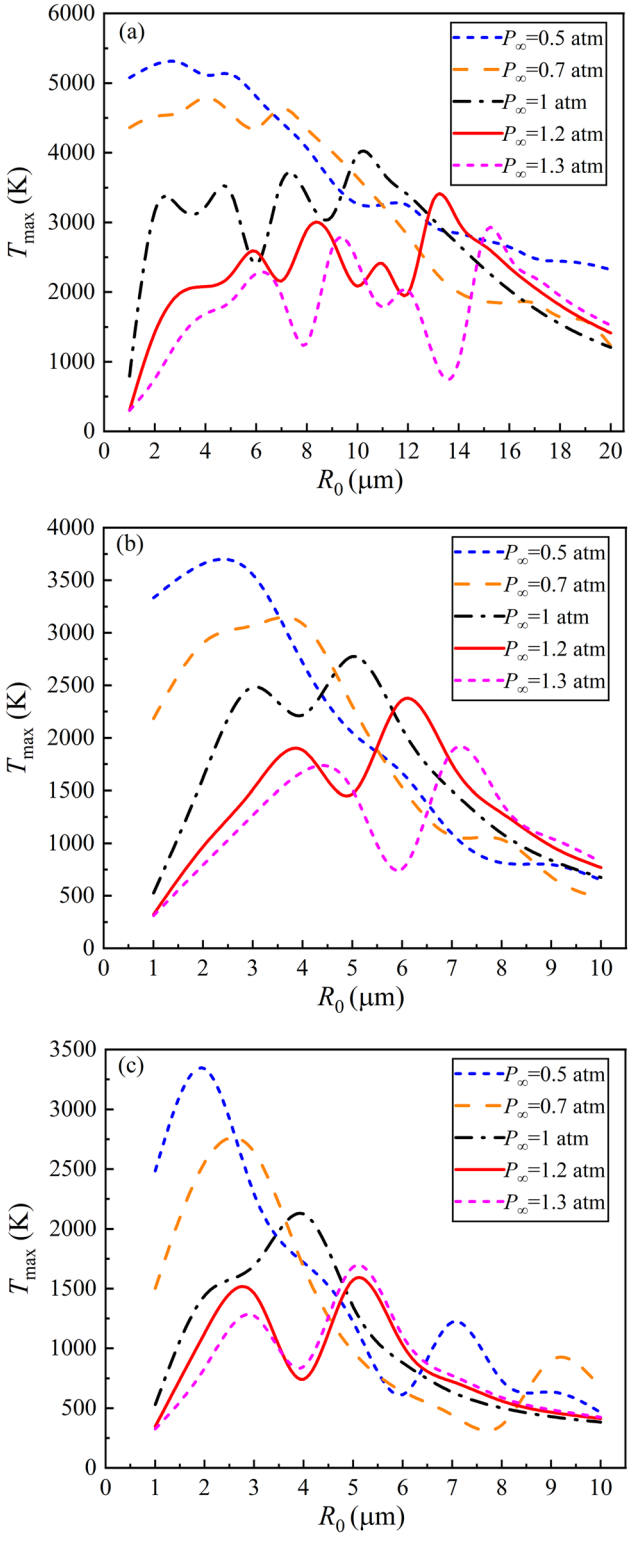

Figure 2: The maximum bubble temperature at the steady state as a function of equilibrium radius under different static pressures (0.5, 0.7, 1, 1.2, and 1.3 atm). The ultrasonic frequencies are 140 kHz (a), 355 kHz (b), and 515 kHz (c). P_A = 1.5 atm.

corresponding to the maximum value changes under different static pressures. When the static pressures are 0.5, 0.7, 1, 1.2, and 1.3 atm, the equilibrium radii corresponding to the maximum temperatures are around 2.62 μm (5,324 K), 4.10 μm (4,785 K), 10.23 μm (4,027 K), 13.23 μm (3,414 K), and 15.26 μm (2,929 K), respectively. When R_0 < 6 μm, the increase of static pressure leads to a decrease in T_{max}. For example, at R_0 = 2 μm, the values of T_{max} are 5,264, 4,523, 3,163, 1,422, and 755 K corresponding to static pressures of 0.5, 0.7, 1, 1.2, and 1.3 atm, respectively.

The calculated results for frequencies of 355 and 515 kHz are shown in Figure 2(b) and (c). It can be observed that the overall variation trend of T_{max} with R_0 is nearly the same, but under the same excitation parameters, T_{max} basically shows a downward trend with the increase of frequency. Similar results were obtained in the study of Dehane *et al.* [19]. In addition, the increase of ultrasonic frequency leads to the increase of R_0 values corresponding to temperatures below 1,000 K, which is the lowest temperature enabling chemical reactions inside the bubble.

The evolution of the molar quantity of H_2 at the steady state as a function of the bubble equilibrium radius (R_0) for five static pressures (0.5, 0.7, 1, 1.2, and 1.3 atm) under different frequencies (140, 355, and 515 kHz) is presented in Figure 3. By changing R_0, Gaussian curves for the molar quantity of H_2 are obtained for all cases. It can be observed that the R_0 values of active bubbles decrease with the increase in static pressure, and this variation trend weakens with the increase in frequency. The specific process can be shown as follows. As static pressure increases from 0.5 to 1.3 atm, the range of active bubbles are 0.61–12.76, 1–12.86, 5.97–15.90, 11.39–17.11, and 12.81–17.57 μm at 140 kHz; 0.75–4.95, 1.16–4.97, 3.31–6.55, 3.73–7.97, and 5.23–8.89 μm at 355 kHz; and 0.98–3.93, 1.93–4.48, 2.61–5.71, 3.22–6.91, and 3.96–6.50 μm. At 140 kHz, the maximum molar amount of H_2 under static pressure of 1 atm is greater than that at 0.7 atm, then 1.2 atm, followed by 0.5 and 1.3 atm. Nevertheless, at 355 and 515 kHz, the above relationship becomes 0.5, 0.7, 1, 1.3, and 1.2 atm.

The molar quantity of ·OH at the steady state as a function of equilibrium radius (R_0) is plotted in Figure 4 under different static pressures (0.5, 0.7, 1, 1.2, and 1.3 atm) at ultrasonic frequencies of 140, 355, and 515 kHz. The overall trend is almost the same as the molar quantity of H_2. Nevertheless, there are some differences between the range of activation bubble radii and the optimal equilibrium radii for ·OH and H_2 production. For instance, at 140 kHz, with static pressures of 1 atm, for ·OH generation, the activation bubble radii range from 5.97 to 15.90 μm, and

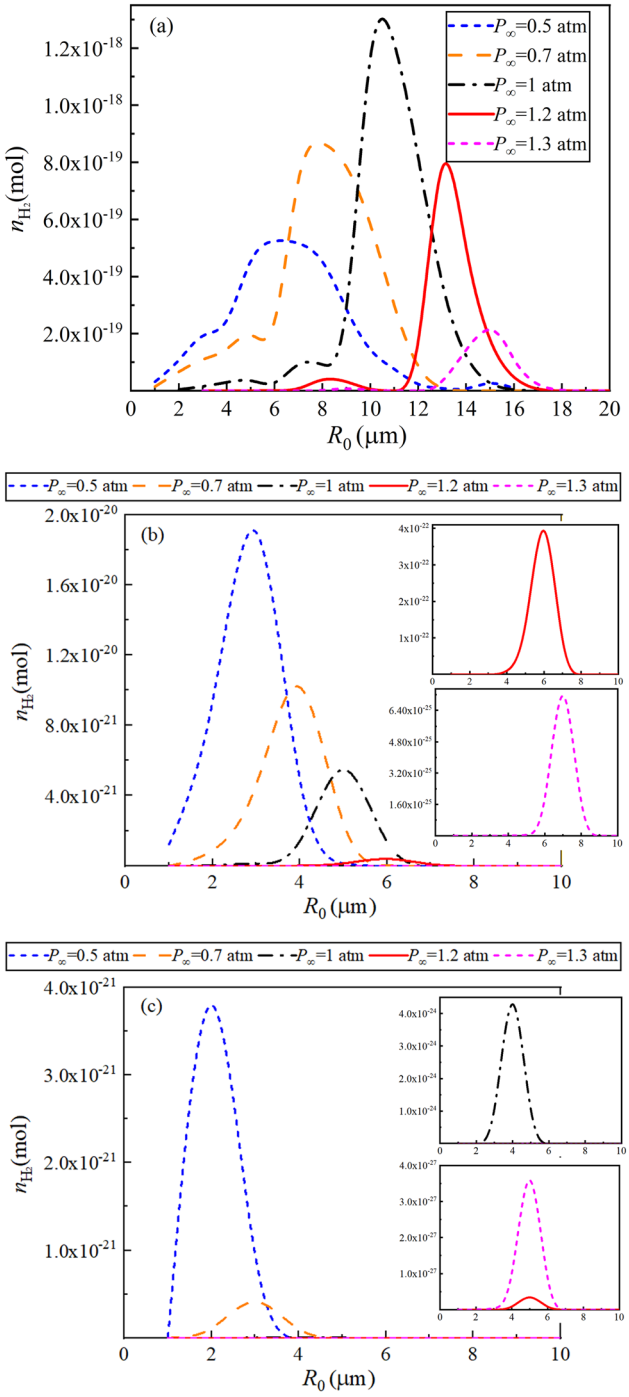

Figure 3: The molar quantity of H_2 at steady state as a function of equilibrium radius under different static pressures (0.5, 0.7, 1, 1.2, and 1.3 atm). The ultrasonic frequencies are 140 kHz (a), 355 kHz (b), and 515 kHz (c). P_A = 1.5 atm.

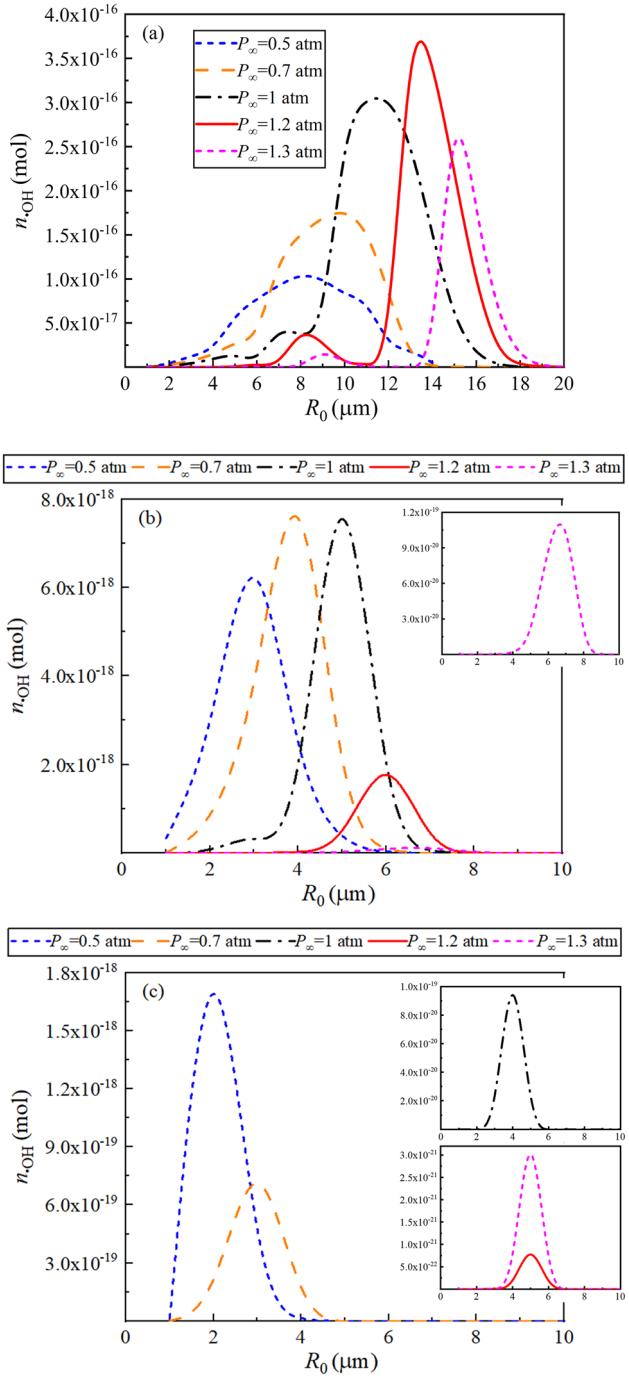

Figure 4: The molar quantity of ˙OH at the steady state as a function of equilibrium radius under different static pressures (0.5, 0.7, 1, 1.2, and 1.3 atm). The ultrasonic frequencies are 140 kHz (a), 355 kHz (b), and 515 kHz (c). P_A = 1.5 atm.

the optimum R_0 = 10.58 μm (1.25×10^{-18} mol), while the two parameters for production are 2.73–17.09 and 11.62 μm (3.04×10^{-16} mol), respectively. These two data for the other conditions can be easily obtained from Figures 3 and 4. In addition, the effect of static pressure on maximum ˙OH production at frequencies 140 and 355 kHz is quite different from its effect on H_2 generation. At a frequency of 140 kHz, the static pressures corresponding to the order of maximum H_2 production from high to low are 1.2, 1, 1.3, 0.7,

and 0.5 atm. At 355 kHz, the relationship is 0.7, 1, 0.5, 1.2, and 1.3 atm. Nevertheless, at 515 kHz, this relationship is the same with respect to that with hydrogen production.

In this study, the effects of equilibrium bubble radius on the maximum temperature, H_2, and ˙OH production at steady state are analyzed under different static pressures with ultrasonic frequencies of 140, 355, and 515 kHz. Previous studies focused on the characteristics of the first main bubble collapse. Compared with the steady state, the collapse time is very short, and the accuracy of the cavitation activity evaluation based on the chemical quality in this state needs further consideration. Therefore, the present study is carried out under a steady state. The increase in bubble temperature enhances the occurrence of chemical reactions, but the above analysis results show that the increase in bubble temperature is not necessarily conducive to the production of H_2 and ˙OH. It is necessary to pay attention to the relationship between the temperature inside the bubble and the chemical production, which has been studied in the study of Merouani *et al.* [18] based on the temperature and chemical production at the bubble collapse. This relationship under steady state will be the focus of our research group in the future.

In the present model, the Keller–Miksis equation is used to describe the radial motion of the bubble, and the effect of liquid compressibility is considered. The characteristics of the mixed gas are described by the state equation of ideal gas. However, the mixed gas is highly compressed during bubble collapse, and gas compressibility needs to be further considered. In addition, the temperature at the bubble wall is the same as at infinity, which is not consistent with the actual situation. Only heat transfer and chemical reaction heat are considered, while mass transfer and unbalanced evaporation and condensation also affect the temperature inside the bubble. Therefore, in a further study, the above factors will be gradually considered, and their influence on the sonochemical process inside the bubble will be analyzed within large parameters.

4 Conclusions

In this study, the model of a single oxygen bubble in water under acoustic excitation is established, and the influence of static pressures (0.5, 0.7, 1, 1.2, and 1.3 atm) with ultrasonic frequencies of 140, 355, and 515 kHz on the sonochemical characteristics inside the bubble at steady state is analyzed numerically. Under different static pressures, with the variation in equilibrium bubble radius, the maximum temperature fluctuates drastically, and the production of H_2 and ˙OH shows Gaussian curve distribution. When the static pressure changes from 0.5 to 1.3 atm, the equilibrium radii corresponding to the maximum temperature are around 2.62, 4.10, 10.23, 13.23, and 15.26 μm, respectively. Different combinations of static pressure and frequency have significant effects on the range of equilibrium bubble radius of cavitation activity and the maximum yields corresponding to the production of H_2 and ˙OH. Consequently, the present study can provide guidance for the design of a sonochemical reactor to improve the production efficacy of H_2 and ˙OH.

Acknowledgments: The authors would like to acknowledge the support given by the 3c-product Intelligent Manufacturing Engineering Technology Research and Development Center of Jiangsu Province (Project No. 201801000010), Jiangsu Province Robot and Intelligent Equipment Engineering Technology Research and Development Center and the teaching reform project of Suzhou Vocational University (Project No. SZDJG-23009).

Funding information: The 3c-product Intelligent Manufacturing Engineering Technology Research and Development Center of Jiangsu Province (Project No. 201801000010), Jiangsu Province Robot and Intelligent Equipment Engineering Technology Research and Development Center and the teaching reform project of Suzhou Vocational University (Project No. SZDJG-23009).

Author contributions: All authors have accepted responsibility for the entire content of this manuscript and approved its submission.

Conflict of interest: The authors state no conflict of interest.

References

[1] Mason TJ. Ultrasonic cleaning: An historical perspective. Ultrason Sonochem. 2016;29:519–23.
[2] Zupanc M, Pandur Ž, Perdih TS, Stopar D, Petkovšek M, Dular M. Effects of cavitation on different microorganisms: The current understanding of the mechanisms taking place behind the phenomenon. A review and proposals for further research. Ultrason Sonochem. 2019;57:147–65.
[3] Fu LP, Zhang GC, Ge JJ, Liao KL, He YF, Wang X, et al. Study on dual-frequency ultrasounds assisted surfactant extraction of oil sands. Fuel Process Technol. 2017;167:146–52.
[4] Lv L, Zhang YX, Wang LY. Effects of liquid compressibility on the dynamics of ultrasound contrast agent microbubbles. Fluid Dyn Res. 2020;52:055507.
[5] Rayleigh L. On the pressure developed in a liquid during the collapse of a spherical cavity. Philos Mag. 1917;34(199):94–8.
[6] Weiss J. Radiochemistry of aqueous solutions. Nature. 1944;153:48–50.

[7] Parke AVM, Taylor DW. The chemical action of ultrasonic waves. J Chem Phys (Resumed). 1956;4442–50.
[8] Didenko YT, Suslick KS. The energy efficiency of formation of photons, radicals and ions during single-bubble cavitation. Nature. 2002;418(6896):394–7.
[9] Wang DL, Liu JY, Qiu SP, Wang JJ, Song GS, Chu BQ, et al. Ultrasonic degradation kinetics and isomerization of 3- and 4-O-caffeoylquinic acid at various pH: The protective effects of ascorbic acid and epigallocatechin gallate on their stability. Ultrason Sonochem. 2022;80:105812.
[10] Matafonova G, Batoev V. Dual-frequency ultrasound: Strengths and shortcomings to water treatment and disinfection. Water Res. 2020;182:116016.
[11] Deng XH, Ni XX, Han JH, Yao WH, Dang YJ, Zhu Q, et al. High-intensity ultrasound modified the functional properties of Neosalanx taihuensis myofibrillar protein and improved its emulsion stability. Ultrason Sonochem. 2023;97:106458.
[12] Wang YC, Li BL, Guo YN, Liu CH, Liu J, Tan B, et al. Effects of ultrasound on the structural and emulsifying properties and interfacial properties of oxidized soybean protein aggregates. Ultrason Sonochem. 2022;87:106046.
[13] Rashwan SS, Dincer I, Mohany A, Pollet BG. The Sono-Hydro-Gen process (Ultrasound induced hydrogen production): Challenges and opportunities. Int J Hydrog Energ. 2019;44(29):14500–26.
[14] Zadeh SH. Hydrogen production via ultrasound-aided alkaline water electrolysis. J Autom Control Eng. 2014;2(1):103–9.
[15] Kamath V, Prosperetti A, Egolfopoulos FN. A theoretical study of sonoluminescence. J Acoust Soc Am. 1993;94(1):248–60.
[16] Yasui K, Tuziuti T, Iida Y, Mitome H. Theoretical study of the ambient-pressure dependence of sonochemical reactions. J Chem Phys. 2003;119(1):346–56.
[17] Merouani S, Hamdaoui O, Rezgui Y, Guemini M. Computer simulation of chemical reactions occurring in collapsing acoustical bubble: dependence of free radicals production on operational conditions. Res Chem Intermediat. 2015;41(2):881–97.
[18] Merouani S, Hamdaoui O, Rezgui Y, Guemini M. Theoretical estimation of the temperature and pressure within collapsing acoustical bubbles. Ultrason Sonochem. 2014;21(1):53–9.
[19] Dehane A, Merouani S, Hamdaoui O. Theoretical investigation of the effect of static pressure on bubble sonochemistry: Special focus on hydrogen and reactive radicals production. Chem Phys. 2021;547:111171.
[20] Kalmár C, Klapcsik K, Hegedűs F. Relationship between the radial dynamics and the chemical production of a harmonically driven spherical bubble. Ultrason Sonochem. 2020;64:104989.
[21] Kalmár C, Turányi T, Gy, Zsély I, Papp M, Hegedűs F. The importance of chemical mechanisms in sonochemical modelling. Ultrason Sonochem. 2022;83:105925.
[22] Eren Z, O'Shea K. Hydroxyl radical generation and partitioning in degradation of methylene blue and DEET by dual-frequency ultrasonic irradiation. J Env Eng. 2019;145(10):04019070.
[23] Benedikt J, Hefny MM, Shaw A, Buckley BR, Iza F, Schäkermann S, et al. The fate of plasma-generated oxygen atoms in aqueous solutions: non-equilibrium atmospheric pressure plasmas as an efficient source of atomic O (aq). Phys Chem Chem Phys. 2018;20(17):12037–42.